Evidence for the strong effect of quenched correlated disorder on phase separation and magnetism in $(La_{1-y}Pr_y)_{0.7}Ca_{0.3}MnO_3$

2010 J. Phys.: Condens. Matter 22 115601

(http://iopscience.iop.org/0953-8984/22/11/115601)

J. Phys.: Condens. Matter **22** (2010) 115601 (5pp) doi:10.1088/0953-8984/22/11/115601

Evidence for the strong effect of quenched correlated disorder on phase separation and magnetism in $(La_{1-y}Pr_y)_{0.7}Ca_{0.3}MnO_3$

V Yu Pomjakushin[1], D V Sheptyakov[1], E V Pomjakushina[2], K Conder[2] and A M Balagurov[3]

[1] Laboratory for Neutron Scattering, ETH Zurich and Paul Scherrer Institut, CH-5232 Villigen PSI, Switzerland
[2] Laboratory for Developments and Methods, PSI, CH-5232 Villigen PSI, Switzerland
[3] Frank Laboratory of Neutron Physics, JINR, 141980 Dubna, Russia

E-mail: Vladimir.Pomjakushin@psi.ch

Received 9 December 2009, in final form 26 January 2010
Published 23 February 2010
Online at stacks.iop.org/JPhysCM/22/115601

Abstract
High resolution neutron diffraction shows that the mesoscopic separation into ferromagnetic (FM) and antiferromagnetic (AFM) phases and the FM transition temperature T_C in the perovskite manganite $(La_{1-y}Pr_y)_{0.7}Ca_{0.3}MnO_3$ strongly depend on the quenched correlated disorder. The different disorder strengths are achieved by different procedures of the sample synthesis and are quantitatively characterized by the microstrain-type diffraction peak broadening. The system shifts to predominantly a one-phase state with smaller T_C as the correlated disorder strength is decreased, supporting the viewpoint that the origin of phase separation in the indicated manganite system is the correlated quenched disorder. The ground state of an ultimately chemically homogeneous sample is FM-like containing about 20% of the AFM minority phase. This FM-like state can be readily transformed to the AFM-like one having <20% of the FM phase by the decrease of the effective charge carrier bandwidth via oxygen isotope substitution.

1. Introduction

The presence of the long scale percolate phase separation in the colossal magnetoresistance (CMR) manganese oxides $A_{1-x}A'_xMnO_3$ (A is rare earth element, A′ is Ca, Sr or Ba) has been attracting special experimental and theoretical attention for a long time. There are two main concepts for the mesoscopically inhomogeneous state in the manganites. One standpoint is that the intrinsic quenched disorder enhances the fluctuations of the competing orders near the original bi-critical point [1–7]. The theoretical calculations in a random field Ising model with quenched correlated disorder [1, 2] show the generation of mesoscopically large clusters of both phases. In another approach, the lattice distortions and the long-range strain [8–11] are the dominant factors controlling the phase separation. The self-organized multiphase coexistence originates purely from the lattice degrees of freedom and is caused by the presence of an intrinsic elastic energy landscape according to the computer simulations [9]. There are also suggestions that the intrinsic quenched disorder and lattice distortions are interrelated in the Mn-substituted half-doped manganites with a low level (1–5%) of Mn substitution [12–14].

The experimental discrimination of the two models is difficult and usually based on concomitant effects. In this paper we give direct evidence in favor of the disorder model by showing that the phase separation is strongly dependent on the strength of the quenched correlated disorder, which can be quantitatively characterized by a microstrain diffraction peak broadening parameter.

The low bandwidth manganite family $(La_{1-y}Pr_y)_{0.7}Ca_{0.3}MnO_3$ (called LPCM hereafter) has the fixed optimal hole

doping $x = 0.3$ and variable A-cation radius $\langle r_A \rangle$ which is linearly connected with the Pr concentration y. The principal effect of decreasing $\langle r_A \rangle$ is a decrease in the Mn–O–Mn bond angle, which leads to the decrease in the electron transfer integral between the Mn ions. The metal–insulator boundary lies at a Pr concentration between $y = 0.86$ and 1.0 [15, 16]. The ground magnetic state in the metallic part of the phase diagram is an incoherent mixture of ferromagnetic metallic FMM and antiferromagnetic insulating AFI mesoscopically large regions [7]. There are two factors controlling the ratio between FMM and AFMI phases. The first one is the effective charge carrier bandwidth W that is decreased as the Mn–O–Mn bond angle is decreased. Due to the strong electron–phonon coupling mediated by the Jahn–Teller effect W is also significantly decreased by the increase in the oxygen mass from ^{16}O to ^{18}O, thus shifting the system also towards an insulating state [7]. The second factor that controls the phase separation is quenched disorder, which modifies the electron transfer integral only locally, but can give rise to the mesoscopically inhomogeneous state in accordance with the model calculations [1, 2].

The quenched disorder in the LPCM system is naturally present due to the dispersion of the A-cation radius, i.e. even an ideally homogeneous statistical distribution of the cations over the crystallographic A position can result in the phase-separated state. It is important to note that, according to elasticity theory, any point defect will create the displacements of neighboring atoms decaying as $1/r^2$ as a function of distance r, creating a correlated disorder region. In real crystals the disorder will be larger due to the presence of different kinds of crystal defects like dislocations, vacancies or composition variance. The defects are classified by their effect on the diffraction peak intensity and width [17]: defects of the first type do not change the diffraction peak widths, but affect their intensity similar to the atomic displacement parameter (ADP), and shift the peak positions. The second type of defects give rise to the peak broadening. Any finite defect is the first type defect and will affect only the integrated peak intensities. To get the line broadening from the finite defects in a 3D crystal the displacements of neighboring atoms have to decrease at a lower rate than $r^{-3/2}$. Any solid solution independent on the partial atomic concentrations will give narrow diffraction peaks [17]. Thus, in the case of an ideal homogeneous statistical distribution of the A cations one expects to have an increase in the ADP and narrow resolution-limited Bragg peak widths. A large scale defect, such as dislocation, is the second type of defect and will create the broadening of the diffraction lines. Possibly some clusterings of particular A cations can act as the second type defects. In a powder diffraction experiment additional broadening can occur also for the first type defects due to the fluctuation of the defect concentration. For the homogeneous solid solutions this broadening is negligibly small but will have a noticeable value in the presence of new phase particles [17]. In our case the clustering of particular A cations can play the role of the 'new phase particle'. We have prepared three types of samples with different correlated quenched disorder strengths that were quantitatively characterized by microstrain-type line broadening and have studied the phase separation effect and magnetism as a function of the disorder. The o-type sample (the nomenclature of sample types is given in section 2) has been studied earlier within a series of $(La_{1-y}Pr_y)_{0.7}Ca_{0.3}MnO_3$ with $y = 0.5$–1.0 [7].

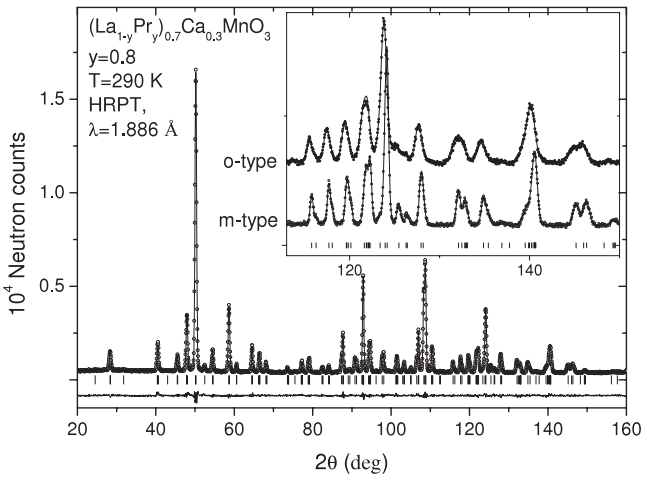

Figure 1. An example of the Rietveld refinement pattern and difference plot of the neutron diffraction data for the $(La_{1-y}Pr_y)_{0.7}Ca_{0.3}MnO_3$ m-type sample with Pr content $y = 0.8$. The inset shows the fragments of diffraction patterns for both o- and m-type samples illustrating much narrower peak widths in the m sample.

2. Samples: experimental details

The samples of $(La_{1-y}Pr_y)_{0.7}Ca_{0.3}MnO_3$ with $y = 0.8$ have been synthesized by a solid state reaction using La_2O_3, Pr_6O_{11}, MnO_2 and $CaCO_3$. The samples, which are denoted as o samples, were calcined at temperatures 1000–1300 °C for 100 h with three intermediate grindings. The final ^{18}O and ^{16}O samples were obtained via respective oxygen isotope exchange in closed quartz tubes in parallel under the controlled gas pressure slightly above 1 bar at 1000 °C during 40 h. The second type is a t sample that has been additionally sintered at higher temperature 1500 °C during 40 h. To further increase chemical homogeneity we applied a procedure similar to the one described in [18] to synthesize the samples that we call m samples. Stoichiometric amounts of the starting materials (15 g) were mixed in an agate mortar and calcined at 950 °C for 12 h (as for standard o samples). At the next step a preliminarily powdered sample was placed in a Fritsch planetary mill (Pulverisette 5, agate balls and grinding bowl) and 15 ml isopropanol was added as the homogenizing liquid. The sample was milled for a total of 4 h at 100 rpm, changing the spinning direction every hour. The obtained suspension was dried at 100 °C and then annealed at 950 °C for 20 h. The sample was milled in the Fritsch mill at the same conditions as in the previous step, dried, pressed into pellets and annealed at 1450 °C for 15 h. Finally the pellets were grounded in an agate mortar, pelletized and sintered at 1500 °C for 12 h.

The chemical homogeneity or composition variance in the solid state synthesis method is expected to be better if the Fritsch planetary mill is used because the minimal comminuted

particle sizes are 0.1 μm, which is significantly smaller than 5–10 μm if ground in a standard agate mortar. The higher sintering temperature is also expected to be a factor improving the homogeneity due to a higher diffusion coefficient.

The ^{18}O samples had 80% of the ^{18}O isotope, measured by the weight gain after oxygen exchange. The control weighing of the ^{16}O sample gave the same mass within an accuracy of 0.03%. The mass of each sample was about 2 g. The oxygen content in all the samples was determined by thermogravimetric hydrogen reduction [19] and amounted to 3.003(5). The ac magnetic susceptibility $\chi(T) = \chi'(T) + i\chi''(T)$ was measured in zero external field with the amplitude of the ac field as 10 Oe and frequency 1 kHz using a Quantum Design PPMS station. Neutron powder diffraction experiments were carried out at the SINQ spallation source at the Paul Scherrer Institute (Switzerland) using the high resolution diffractometer for thermal neutrons HRPT [20] (neutron wavelength $\lambda = 1.866, 1.494$ Å) and the DMC diffractometer [21] situated at a supermirror-coated guide for cold neutrons at SINQ ($\lambda = 2.56$ Å). All the temperature scans were carried out on heating. The refinements of the crystal and magnetic structure parameters were carried out with the FULLPROF [22] program, with the use of its internal tables for scattering lengths and magnetic form factors.

3. Results and discussion

The crystal structure at all temperatures is well refined in single phase in space group *Pnma* with the standard for these compounds model [23]. An example of the Rietveld refinement pattern and the difference plot of neutron diffraction is shown in figure 1. The structure disorder can be characterized by atomic displacement parameters (ADP) and microstrain-type line broadening. We indeed observe large ADP $B = 0.90(2), 0.50(2), 1.00(3)$ Å^2 for the A cation, Mn and oxygen atoms, respectively, in $(La_{1-y}Pr_y)_{0.7}Ca_{0.3}MnO_3$ ($y = 0.8$). The B values are more than two times larger than in a 'defect-free' isostructural $LaMnO_3$ that has $B = 0.34(2), 0.21(3), 0.47(3)$ Å^2, respectively [24]. Both $LaMnO_3$ and LPCM compounds have the same Jahn–Teller-type (JT) transition at high temperature (800 K) from pseudo-cubic to the antiferrodistortive orbital ordered state with a completely filled z^2-type orbital at room temperature [7]. The enhanced ADP are naturally expected due to the distribution of the cations with significantly different atomic radii over the A positions and the presence of 30% of non-JT-active manganese ions Mn^{4+} that can also act as defects. In all three types of samples with $y = 0.8$ the ADP values are the same within experimental error bars, implying that the point-like quenched disorder does not depend on the sample type. The parameter characterizing the correlated quenched disorder is the microstrain-type line broadening parameter $(\delta d/d)_{st}$ that has been determined from the refinement of the diffraction patterns as described in section III-B of [7]. The refined values of $(\delta d/d)_{st}$ are shown in table 1. For all samples, the apparent crystalline sizes L are refined to values larger than 5×10^3 Å with the error bars of the same order of magnitude, giving only a small contribution to the line broadening (assuming $1/L = 0$

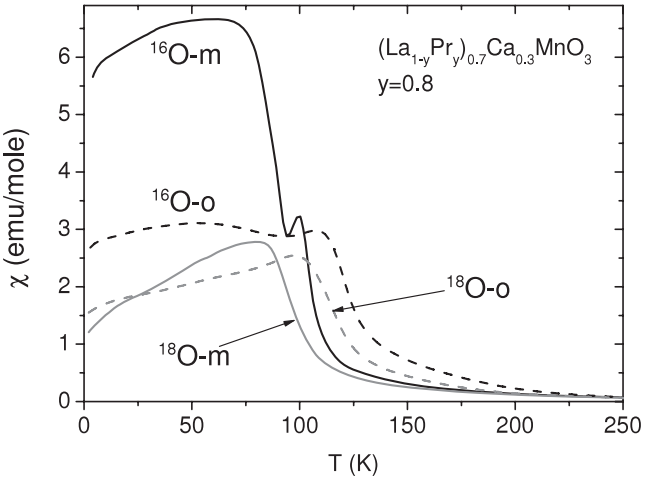

Figure 2. Real χ' part of the ac magnetic susceptibilities are shown as a function of temperature for $(La_{1-y}Pr_y)_{0.7}Ca_{0.3}MnO_3$ samples with Pr content $y = 0.8$. M and o samples are shown by solid and dashed lines, respectively. ^{18}O-substituted samples are shown by gray lines.

Table 1. The microstrain line broadening parameter $(\delta d/d)_{st}$ determined from NPD at room temperature in $(La_{1-y}Pr_y)_{0.7}Ca_{0.3}MnO_3$ samples. The number in the sample name stands for $y \times 100$ and the letter denotes the sample type. All the samples are with natural oxygen isotope ^{16}O except the 80-m18 that is ^{18}O-substituted. The data for samples 80-o and 20-o are from [7]. The Curie transition temperatures T_C and rms variance of the Gaussian distribution of the transition temperatures δT_C were determined from the fits of neutron diffraction intensities $I(T)$ [7]. m_F and m_A are effective ferro- and antiferromagnetic moments at $T \leqslant 15$ K determined by NPD.

Sample	$10^4 \times \delta d/d$	T_C (K)	δT_C (K)	m_A, μ_B	m_F, μ_B
80-o	26(2)	120(2)	23(2)	1.65(2)	3.03(2)
80-t	22(3)	106(1)	11(2)	1.01(5)	3.21(4)
80-m	7.0(1.8)	90.4(4)	3.2(4)	0.93(3)	3.40(2)
80-m18	8.8(1.4)	85(2)	3.3(4)	2.05(2)	1.47(3)
20-o	26(2)	240.3(1)	0	0.15(2)	3.57(2)
20-t	12(3)	223(1)	0	—	3.49(5)

increases the refined microstrain values by less than 10%). One can see that the additional thermal treatment (t samples) slightly decreases the microstrain, whereas the use of the planetary mill for the m samples drastically reduces $(\delta d/d)_{st}$ down to 7×10^{-4}, which is illustrated by the inset of figure 1. M samples have probably an ultimate chemical homogeneity because the microstrain is close to the one expected from the twin tension due to the high temperature pseudo-cubic–orthorhombic structure transition [7]. T and o samples can have some clustering of the La/Ca/Pr atoms because in the solid state synthesis the high temperature reaction takes place between small solid pieces of the comminuted materials.

The ac magnetic susceptibility as a function of temperature $\chi(T)$ for both o and m samples is shown in figure 2. One can see that the $\chi(T)$ dependence in the milled m sample possesses quite a sharp feature around 100 K and significantly larger absolute values of χ'. The reason for the different behaviors of m and o samples is the different

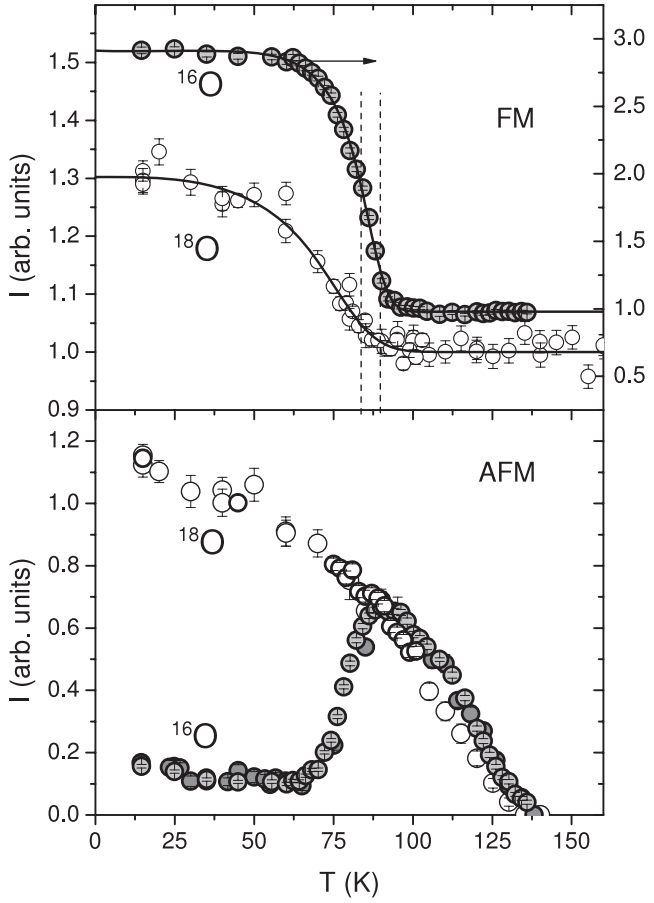

Figure 3. Temperature dependences of the integrated intensities of the selected ferro- (FM) and antiferromagnetic (AFM) diffraction peaks in the $(La_{1-y}Pr_y)_{0.7}Ca_{0.3}MnO_3$ m samples $y = 0.8$. The data collected on heating. ^{16}O and ^{18}O samples are shown by closed and open symbols, respectively. The lines are fits to the formula described in [7]. Note that the FM intensity of the ^{18}O sample is significantly smaller than the ^{16}O one and has a different y axis. The vertical lines indicate the refined positions of the FM transition temperatures.

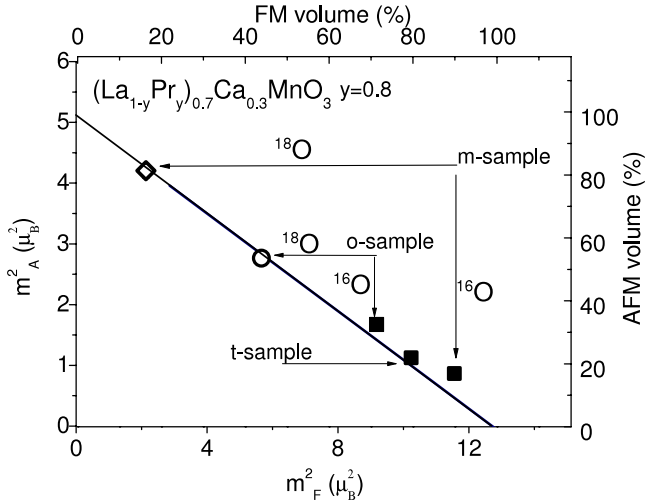

Figure 4. Effective antiferromagnetic (AFM) m_A^2 as a function of the effective ferromagnetic (FM) moment m_F^2 for the $(La_{1-y}Pr_y)_{0.7}Ca_{0.3}MnO_3$ samples with $y = 0.8$. The top x and right y axes show respectively FM and AFM phase fractions. The closed and open symbols represent the ^{16}O and ^{18}O samples, respectively. Three types of samples, o, t and m samples, with different strengths of correlated quenched disorder are indicated by arrows. The data for o samples and the straight line, which is a fitted result, are taken from [7].

proportion between the FM and AFM fraction as we show below. An important consequence of this 'sample effect' for the manganite physics is that the temperature dependences of various macroscopic quantities, such as magnetic susceptibility or electrical resistivity, will not be reproducible in different experimental works if the quenched correlated disorder is not controlled. Hence, different experimental data cannot be easily compared with each other and compared with the theoretical predictions. Note that all structure parameters of o and m samples (e.g. bond lengths and angles) are the same within the error bars. A similar observation was reported for the charge-ordered $Nd_{1/2}Sr_{1/2}MnO_3$, where the microstrain and phase separation on FM and AFM phases below 150 K depended on the sample preparation procedure [25].

The magnetic phase-separated state consists of the AFM pseudo-CE phase with the Mn spin directed along b and the FM phase with the Mn spin in the ac-plane, similar to the one reported in [26]. The FM transition temperatures T_C (table 1) were determined from the magnetic Bragg peak intensities $I(T)$ (figure 3) by the fitting procedure described in [7]. One can see that the transition temperatures T_C and the transition width δT_C are decreased as the microstrain $(\delta d/d)_{st}$ is decreased. The counterintuitive decrease in T_C, however, finds its explanation in the 3D correlated disorder double exchange model [27]. The calculations show that at hole densities lower than $x = 0.5$ where the couplings are strongly inhomogeneous, T_C in the inhomogeneous system is larger than in the homogeneous one [27]. In the case of uncorrelated Anderson disorder the effect would be opposite, i.e. the inhomogeneous system would have a lower transition temperature. To further prove this effect we have additionally prepared and studied an $(La_{1-y}Pr_y)_{0.7}Ca_{0.3}MnO_3$ ($y = 0.2$) t sample that is located in the ferromagnetic metallic part of the phase diagram [7]. We have found that it shows essentially the same behavior (table 1): after the additional annealing of the t sample the transition temperature T_C is decreased together with the microstrain $(\delta d/d)_{st}$.

Figure 4 shows the fractions of the FM and AFM phases in the samples of $(La_{1-y}Pr_y)_{0.7}Ca_{0.3}MnO_3$ $y = 0.8$ calculated from the effective moments from table 1. The straight line is taken from [7] and represents a fit to the experimental effective moments $m_A^2(m_F^2)$ for the whole series of o samples with $y = 0.2$–1. One can see that the ^{16}O samples gradually move along this straight line towards the FM state as the strength of the disorder is decreased (from o to t and to the m sample). This shows that the stronger the correlated disorder the larger the separation into FM and AFM phases. Additional evidence comes from the effect of oxygen isotope substitution also shown in figure 4. A decrease in the effective bandwidth in the ^{18}O samples shifts the phase balance toward the AFM state, as expected. But, in addition, the low defect ^{18}O m sample displays a much larger AF fraction in comparison with the o samples, i.e. again the sample with minimal correlated

disorder tends to be in the single-phase state. However, even the ultimately chemically homogeneous m samples still contain 10–20% of the minority phase, justifying that the mesoscopically inhomogeneous magnetic state is an intrinsic property of $(La_{1-y}Pr_y)_{0.7}Ca_{0.3}MnO_3$.

One could suggest that the single crystals might be the most suitable candidates with the best homogeneity to verify further the effects of correlated quenched disorder. Due to the high melting temperatures of LPCM a reasonably large crystal can be grown only by the traveling solvent floating zone technique (TSFZ). A single crystal of $(La_{1-y}Pr_y)_{0.7}Ca_{0.3}MnO_3$ ($y = 0.7$) grown by the TSFZ has been studied by a magneto-optical imaging technique [28]. Figure 4 of the above reference nicely shows the presence of mesoscopic phase separation into FM and AFM phases at $T = 34$ K. From this figure, one could estimate that the fraction of the AFM phase is more than 20%. Thus the phase separation is even more pronounced than in the ultimately homogeneous powdered m samples, implying that the defect concentration in the crystal is not smaller. It is known that the crystals grown by the TSFZ or similar technique from melt can be inhomogeneous and contain many defects mainly due to large temperature gradients [29]. The polycrystalline materials that are sintered at high temperatures and slowly cooled down might have less defects than the single crystals grown by TSFZ, provided that the pulverized particle sizes are small enough.

4. Conclusions

We have studied the effect of correlated quenched disorder on the phase separation in perovskite manganese oxide $(La_{1-y}Pr_y)_{0.7}Ca_{0.3}MnO_3$. The different disorder strengths were achieved by different procedures of sample synthesis and quantitatively characterized by microstrain-type diffraction peak broadening. We have found that the decrease of the correlated disorder pushes the system to predominantly one phase and decreases the ferromagnetic Curie temperature in accordance with the theoretical predictions [2, 27]. The ground state of an ultimately chemically homogeneous sample (i.e. with statistical distribution of La/Pr/Ca cations over the A position) is still a phase-separated one but with the dominant magnetic phase occupying 80–90% of the volume. The dominant phase is the ferromagnetic one for the sample with natural oxygen, but it can be readily transformed to the antiferromagnetic phase by the decrease of the effective charge carrier bandwidth via $^{16}O/^{18}O$-oxygen isotope substitution.

An important consequence of the effect of the correlated disorder for the manganite physics is that the temperature dependences of various macroscopic quantities such as magnetic susceptibility or electrical resistivity will not be reproducible in different experimental works and cannot be correctly compared with the theoretical predictions if the correlated quenched disorder strength is not controlled.

Acknowledgments

This study was performed at the Swiss neutron spallation source SINQ at the Paul Scherrer Institute PSI (Villigen, PSI). Financial support by the NCCR MaNEP project is gratefully acknowledged.

References

[1] Burgy J, Mayr M, Martin-Mayor V, Moreo A and Dagotto E 2001 *Phys. Rev. Lett.* **87** 277202
[2] Burgy J, Moreo A and Dagotto E 2004 *Phys. Rev. Lett.* **92** 097202
[3] Alonso J L, Fernandez L A, Guinea F, Laliena V and Martin-Mayor V 2002 *Phys. Rev.* B **66** 104430
[4] Blake G R, Chapon L, Radaelli P G, Argyriou D N, Gutmann M J and Mitchell J F 2002 *Phys. Rev.* B **66** 144412
[5] Akahoshi D, Uchida M, Tomioka Y, Arima T, Matsui Y and Tokura Y 2003 *Phys. Rev. Lett.* **90** 177203
[6] De Teresa J M, Algarabel P A, Ritter C, Blasco J, Ibarra M R, Morellon L, Espeso J I and Gómez-Sal J C 2005 *Phys. Rev. Lett.* **94** 207205
[7] Pomjakushin V Y, Sheptyakov D V, Conder K, Pomjakushina E V and Balagurov A M 2007 *Phys. Rev.* B **75** 054410
[8] Littlewood P 1999 *Nature* **399** 529–31
[9] Ahn K H, Lookman T and Bishop A R 2004 *Nature* **428** 401–4
[10] Podzorov V, Kim B G, Kiryukhin V, Gershenson M E and Cheong S W 2001 *Phys. Rev.* B **64** 140406(R)
[11] Sharma P A, Kim S B, Koo T Y, Guha S and Cheong S W 2005 *Phys. Rev.* B **71** 224416
[12] Yaicle C, Fauth F, Martin C, Retoux R, Jirak Z, Hervieu M, Raveau B and Maignan A 2005 *J. Solid State Commun.* **178** 1652–60
[13] Yaicle C, Frontera C, Garcia-Munoz J L, Martin C, Maignan A, Andre G, Bouree F, Ritter C and Margiolaki I 2006 *Phys. Rev.* **74** 144406
[14] Frontera C, Garcia-Munoz J L, Beran P, Bellido N, Margiolaki I and Ritter C 2008 *Chem. Mater.* **20** 3068–75
[15] Hwang H Y, Cheong S W, Radaelli P G, Marezio M and Batlogg B 1995 *Phys. Rev. Lett.* **75** 914–7
[16] Babushkina N A, Belova L M, Taldenkov A N, Chistotina E A, Khomskii D I, Kugel K I, Gorbenko O Y and Kaul A R 1999 *J. Phys.: Condens. Matter* **11** 5865–73
[17] Krivoglaz M A 1996 *X-Ray and Neutron Diffraction in Nonideal Crystals* (Berlin: Springer)
[18] Collado J, Frontera C, Garcia-Munoz J, Ritter C, Brunelli M and Aranda M 2003 *Chem. Mater.* **15** 167–74
[19] Conder K, Zhao G M and Khasanov R 2002 *Phys. Rev.* B **66** 212409
[20] Fischer P, Frey G, Koch M, Koennecke M, Pomjakushin V, Schefer J, Thut R, Schlumpf N, Buerge R, Greuter U, Bondt S and Berruyer E 2000 *Physica* B **276–278** 146–7 http://sinq.web.psi.ch/hrpt
[21] Fischer P, Keller L, Schefer J and Kohlbrecher J 2000 *Neutron News* **11** 19
[22] Rodriguez-Carvajal J 1993 *Physica* B **192** 55–69
[23] Balagurov A M, Pomjakushin V Y, Sheptyakov D V, Aksenov V L, Babushkina N A, Belova L M, Gorbenko O Y and Kaul A R 2001 *Eur. Phys. J.* B **19** 215–23
[24] Rodriguez-Carvajal J, Hennion M, Moussa F, Moudden A H, Pinsard L and Revcolevschi A 1998 *Phys. Rev.* B **57** R3189–92
[25] Woodward P, Cox D, Vogt T, Rao C and Cheetham A 1999 *Chem. Mater.* **11** 3528–38
[26] Balagurov A M, Pomjakushin V Y, Sheptyakov D V, Aksenov V L, Fischer P, Keller L, Gorbenko O Y, Kaul A R and Babushkina N A 2001 *Phys. Rev.* B **64** 024420
[27] Bouzerar G and Cepas O 2007 *Phys. Rev.* B **76** 020401(R)
[28] Tokunaga M, Tokunaga Y and Tamegai T 2004 *Phys. Rev. Lett.* **93** 037203
[29] West A R 2003 *Solid State Chemistry and its Applications* (New York: Wiley)